Hindawi
Mathematical Problems in Engineering
Volume 2019, Article ID 9048025, 13 pages
https://doi.org/10.1155/2019/9048025

Research Article

Numerical Analysis of the Influence of Electrode Inclination on Temperature Distribution during GMAW Overlaying

Jerzy Winczek,[1] **Marek Gucwa**,[1] **Miloš Mičian**,[2] **and Krzysztof Makles**[1]

[1]*Częstochowa University of Technology, 42-201 Częstochowa, Poland*
[2]*University of Žilina, Univerzitná 1, 010 26 Žilina, Slovakia*

Correspondence should be addressed to Jerzy Winczek; winczek@gmail.com

Received 29 December 2018; Revised 25 February 2019; Accepted 11 March 2019; Published 26 March 2019

Academic Editor: Alberto Campagnolo

In the work, an analysis of the influence of electrode inclination on the distribution of temperature in the weld overlaying has been conducted. In the analytical description of the temperature field, a volumetric heat source model with an inclined axis with respect to the direction of surfacing was adopted. In the numerical simulation, the own theoretical model of heat source, algorithm, and program performed in the Borland Delphi environment were used. In the calculation examples, different electrode inclination angles were adopted in relation to the welded plate, in the direction of surfacing, opposite to the direction of welding, and perpendicular to the weld bead.

1. Introduction

In welding processes (e.g., joining, overlaying, rebuilding, and cutting), it is often occurring that the electrode is inclined to the material. Many researches indicate the electrode tilt input on the shape and dimensions of the weld and on the temperature field during welding (surfacing, rebuilding). When welding with the electrode tilted according to its motion, the thickness of the fusion zone decreases and the arc penetrates deeper, while at the opposite inclination, the penetration of the weld decreases with increasing its width.

In the modeling of technological processes, the temperature fields caused by mobile heat sources are taken into account. In some technologies, physical phenomena caused by the action of heat sources are the essence of these processes. Jiang et al. [1] developed a full three-dimensional thermomechanical finite element model to simulate the step-by-step multipass welding process. Nonlinearities associated with welding, such as a moving heat source, material deposition, temperature-dependent material properties, latent heat, and large deformation, were taken into account. Numerical simulations were performed for a butt-welded joint of plate made GMA method described in [2], obtaining odd agreements with the results of experimental studies. Wang et al. [3] proposed 3D string heat source model was developed to simulate the thermal process for gas metal arc welding (GMAW) with a new transient solution of heat transfer. The moving welding heat input during GMAW welding process was presented with a moving 3D string heat source model made up of a group of elementary point heat sources along the moving coordinate axes. Hildebrand et al. [4] carried out numerical simulations of the temperature field in the analysis of the impact of the TIG-dressing of weld transition on improving of the fatigue strength of a welded connection by reducing the sharpness of the notch possible. Kang and Cho [5] solved temperature field in welding model using GTA method taking into consideration filler wire. Ghosh et al. [6] presented (using analytical method) on thermal behavior during submerged arc welding considering an oval shaped Gaussian heat source. Mahapatra et al. [7] performed three-dimensional analysis (using the FEM method) of the temperature field in single-pass shielded arc welding butt joints. Filler material deposition was also simulated. The analysis of temperature field using Goldak's double-ellipsoidal heat source model and Sysweld program, for two overlapping beads on a substrate steel plate, has been conducted by Joshi et al. [8]. The results of numerical simulations have been experimentally verified using the FCAW process. Franco et al. [9] provided a methodological approach for analytical modelling of deep penetration laser beam welding (LBW)

of stainless steels and its experimental verification. Piekarska and Kubiak [10] described mathematical and numerical models of thermal phenomena developed for computational analysis of the laser–arc hybrid welding process with verified by experimental result. In [11], a numerical simulation of PAC (Plasma Arc Cutting) process by ANSYS software for gaining the temperature field of stainless steel, the effect of parameter variation on temperature field, and process optimization for different cases of plasma and shielding gases are done. Li et al. [12] developed an evolutionary keyhole-mode heat transfer model for continuous PAW (Plasma Arc Welding), in which a double-elliptical heat source was set up on top surface and a developing conical heat source below, which is closely related to keyhole depth by volume of fluid method. Haghpanahi et al. [13] proposed three-dimensional analytical model of temperature field in FSW (Friction Stir Welding) based on Green's function. Jiang and Dai [14] carried out three-dimensional thermodynamic analysis of simply supported high strength and low alloy rectangular steel plates under laser shock processing. In some technologies, thermal processes are used in conjunction with other methods of processing. In [15], a mathematical model of the coating formation by electric contact surfacing was proposed. The method of numerical recurrent solution of the finite-difference form of static equilibrium conditions of the selected elementary volume of coating has been used. Feng et al. [16] presented a three-dimensional (3D) analytical model for the temperature field in the hybrid laser-waterjet micro-machining process, taking into account the formation of laser-induced plasma in water, bubble formation, and the laser refraction at the air-water interface. In the machining processes, the release of heat is the result of the tool friction with the material being processed. Murčinková and Vasilko [17] conducted an analysis of the thermophysical aspects of the chip processing, namely, the impact of the cutting speed on the heat flow in the cutting zone, treating the cutting tool as a moving heat source. In all of these cases, the heat source moves relative to the workpiece.

Modelling of temperature field in welding processes dominates two approaches: analytical (most frequently based on integral transformations and Green's function method) and numerical (in which the finite-difference methods, infinitesimal balances, and FEM are commonly used). First attempts to describe the temperature field in the welding process and related processes were undertaken in the middle of the last century by Rosenthal [18] and Rykalin [19]. Rosenthal [18] was the first who obtained the equation of the temperature distribution for quasi-steady state for different heat source models: point and linear in the form of a segment parallel to the axis of the weld. Next Rykalin [19] adopted a heat source in the form of a perpendicular segment. Eagar and Tsai [20] modified Rosenthal's model including two-dimensional Gaussian distributed heat source and developed solution to moving heat source in a semi-infinite steel plate. Double-ellipsoidal three-dimensional heat source was first introduced by Goldak [21]. The finite elements method was used to determine temperature field in sheet weld. The analytical solution to temporary temperature field of fillet weld was presented by Jeong and Cho [22] using conformal techniques of mapping. On the other hand, solution to the temperature field in massive body caused by half-elliptical double-ellipsoidal volumetric heat source was presented by Nguyen at al. [23].

Despite many works describing the temperature field in welding processes, a continuous search for models of heat sources and temperature fields that would reproduce temperature distributions as close as possible to the actual is still continued. Gu et al. [24] proposed the isoparametric transformation and computer graphics technique in conjunction with the optimization method to determine the double-ellipsoidal heat source model parameters. In [25], based on the configuration feature of keyhole PAW welds, a combined heat source model for the numerical analysis of temperature fields in keyhole PAW process has been proposed. With this adaptive heat source model, finite-element analysis of temperature profile in keyhole PAW was conducted and the weld geometry was determined. Jia et al. [26] developed new method to accurately estimate heat source parameters in welding simulation, obtained with both the multiple regression analysis and the partial least-squares regression analysis between heat source parameters and welding pool geometry. Mikami et al. [27] used two types of heat source models, "weaving" and "quasi-weaving" to simulation of temperature field and residual stress distribution in weaving welds. The obtained results of numerical calculations suggest that the modeling of a weaving heat source using a quasi-weaving model requires adjustment of the temperature distribution. In [28], the double-ellipsoidal distribution is extended to a double-ellipsoidal-conical heat power density model in order to accurately describe transient temperature fields for a wider range of geometries and welding processes. The new extended model was validated through comparing predicted welding thermal cycles with those measured for a single-pass electron beam weld, as well as those measured in a multipass narrow groove gas-tungsten-arc weld. The experimental verification of the method showed satisfactory results. Nasiri and Enzinger [29] proposed an analytical description of the temperature field in fillet welds using the adaptive function method. The adaptive function method is a general approach to solving a partial differential equation based on nondimensional parameters and developing an adaptive function by manipulating Rosenthal's equation. In [30] developed a multiple model adaptive inverse method to estimate the heat source intensity of nonlinear heat transfer system with a moving heat source. In the whole motion space of heat source, the nonlinear heat transfer system is divided into several linearized subspaces, and a corresponding linear prediction submodel for the temperature at the measurement point is established for each subspace.

Surfacing (rebuilding) by welding is a process commonly used to regenerate or repair damaged parts or to obtain hard-wearing surfaces (hardfacing). In this process, the tilt of the electrode toward to the movement direction is often used. In addition to the perpendicular electrode to the surface, two techniques are used (Figure 1): (a) with the electrode inclination toward the direction of motion; (b) with the electrode inclined in the direction opposite to its movement.

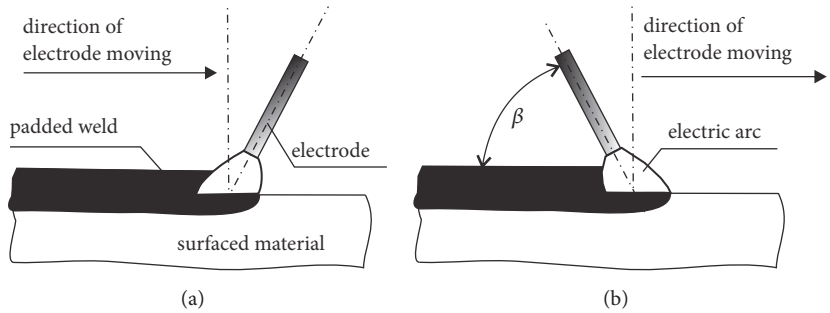

Figure 1: Scheme of weld surfacing with a tilted electrode: (a) electrode inclined in the direction opposite to its movement; (b) electrode inclination toward the direction of motion.

Many works indicate the electrode tilt input on the shape and dimensions of the weld and on the temperature field during welding (surfacing, rebuilding). Klimpel et al. [31], pointed out that by changing a direction and inclination angle of the GMA welding torch and the values of the power per unit length of weld, one can influence the shape and properties of the welds. When welding with the electrode tilted according to its motion, the thickness of the fusion zone decreases and the arc penetrates deeper, while at the opposite inclination, the penetration of the weld decreases with increasing its width [32]. Investigations into the effect of the padding method on the shape of the overlay bead and the content of the base material in the weld [33] showed that with a change in the direction and the angle of inclination of the holder and, also, depending on the rate of deposition, the depth of penetration is altered. Experimental tests of X2CrTi12 steel surfacing by welding (GMA and GMA Puls) presented in [34] showed that the angle of inclination of the electrode influences the shape of the padding weld. Angle values below 90° allow for deeper penetration and narrower padding, while above this value, the depth of penetration is smaller and padding weld wider.

Kumar and Debroy [35] developed a three-dimensional numerical heat-transfer and fluid-flow model to capture the effects of the tilt angle of the fillet joint and on the temperature profiles, weld pool shape, weld pool free surface profile, and thermal cycles during GMA welding in spray mode. In work [36] by Hongyuan et al., an extended Goldak model was proposed, taking into account the inclination of the vertical source axis, and this model was used to determine the temperature field using FEM (Finite Element Method). Developed model was used for calculation of weld pool cross-section configuration during twin wire welding. The influence of torch angles on distribution of temperature and geometry of weld bead during TIG-MIG hybrid welding was analyzed using FEM by Chen et al. [37]. The proposed heat source algorithm allowed predicting the welding process, regardless of whether the electrode gun is slanted backwards or forward to the welding direction. In the work of Gosh et al. [38], the model of moving tilted volumetric heat source was presented. The temperature field was analyzed for different angles of inclination, with little difference in value, only one way of the electrode inclination and for selected points. The effect of changing the angle of the electrode inclination on the temperature distribution was not analyzed.

The authors of this paper propose an alternative model and have made a theoretical analysis of the temperature field for diametrically different values of the inclination angle of the heat source. Computations were made for entire cross-sections of the welded element: perpendicular and longitudinal, as well as on the surface of the workpiece. This approach allows for a qualitative assessment of changes in temperature distributions caused by the varying inclination of the heat source.

2. Analytical Solution of Temperature Field for the Tilted Heat Source Model

In order to describe the temperature field in an isotropic and homogeneous body, the solution of the differential heat conduction equation was used, resulting from the law of conservation of energy [39]. Based on earlier analytical solution [40] for volumetric heat source with an axis perpendicular to the heated object, the temperature field in a semi-infinite body model of the surfaced steel element taking into account the electrode inclination is proposed. As in other analytical considerations, the latent heats of phase transitions (both solid and liquid) are omitted and Joule heat is ignored. Similarly to the known analytical solutions of the differential equation of heat conduction, the thermophysical material properties as independent of temperature have been assumed. In the calculations, the volumetric heat source model with an inclined axis has been used. Heat power along its diameter is defined by Gaussian function characterized by the average radius r_B (Figure 2), for which the power equals

$$q\left(r_{\mathrm{B}}\right) = \frac{q_{max}}{e} \tag{1}$$

where q_{max} means the maximum power of the distribution.

The power of the source in relation to depth is determined by the parabolic function (Figure 3):

$$q\left(z\right) = q_{max}\left(1 - \left(\frac{z}{z_g}\right)^2\right) \tag{2}$$

where

$$z_g = z_0 \cos\gamma \tag{3}$$

z_g [m]: depth of heat source deposition; z_0 [m]: the maximum length deposition of the heat source (by $\gamma = 0$).

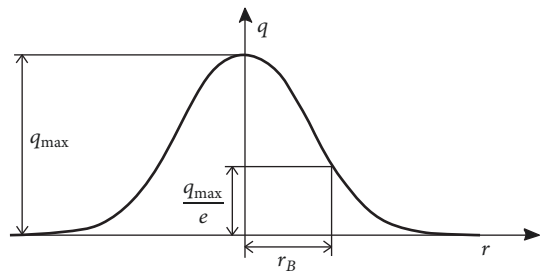

Figure 2: Gaussian power distribution along its diameter.

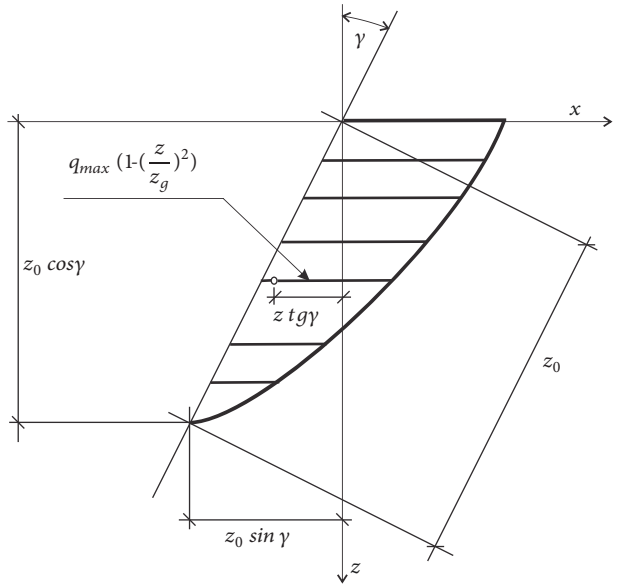

Figure 3: Parabolic change in relation to depth.

The temperature during single-pass arc overlaying welding (Figure 4) in time $\leq \tau_t$, where τ_t is defined by

$$\tau_t = \frac{l}{v} \tag{4}$$

and will be determined by the equation

$$\theta(x,y,z,\tau) - \theta_0 = \frac{3\dot{q}}{16c\rho(\pi a)^{1.5} z_g} \exp\left(-\frac{\xi v}{2a} - \frac{v^2\tau_0}{4a}\right) \cdot \int_0^t \frac{1}{(\tau'' + \tau_0)(\tau'')^{0.5}} \exp\left(-\frac{\xi^2 + (y-y_0)^2}{4a(\tau'' + \tau_0)} - \frac{v^2\tau''}{4a}\right)(\psi_1(z) + \psi_2(z))\, d\tau'' \tag{5}$$

whereas after application of a whole welding pad (for time $\tau > \tau_t$), the relationship for the temperature calculation is defined by

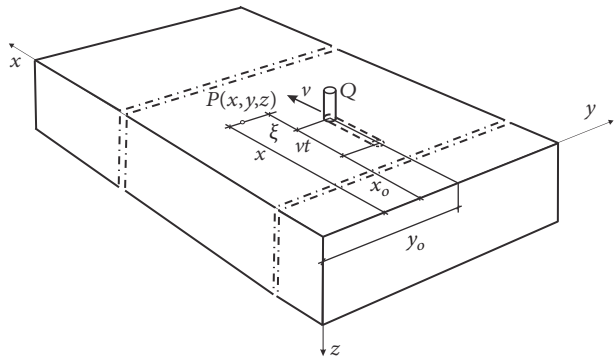

Figure 4: Single-pass arc overlaying welding scheme.

$$\theta(x,y,z,\tau) - \theta_0 = \frac{3\dot{q}}{16c\rho(\pi a)^{1.5} z_g} \cdot \int_0^\tau \frac{1}{(\tau + \tau_0 - \tau')(\tau - \tau')^{0.5}} \cdot \exp\left(-\frac{(x - v\tau' - x_0)^2 + (y - y_0)^2}{4a(\tau + \tau_0 - \tau')}\right) \cdot (\psi_3(z) + \psi_4(z))\, d\tau' \tag{6}$$

where

$$\psi_1(z) = \frac{D_H^{0.5}}{8A_H^{2.5} z_g^2} \exp\left(-\frac{A_H z_g^2 + B_H z_g + C_H}{D_H}\right) \cdot \left\{2A_H^{0.5} D_H^{0.5}\left[B_H\left(-1 + \exp\left(\frac{A_H z_g^2 + B_H z_g}{D_H}\right)\right) + 2A_H z_g\right] + \exp\left(\frac{(2A_H z_g + B_H)^2}{4A_H D_H}\right)\pi^{0.5}\left[-4A_H^2 z_g^2 + B_H^2 + 2A_H D_H\right]\left[\operatorname{erf}\left(\frac{B_H}{2A_H^{0.5} D_H^{0.5}}\right) - \operatorname{erf}\left(\frac{2A_H z_g + B_H}{2A_H^{0.5} D_H^{0.5}}\right)\right]\right\} \tag{7}$$

$$\psi_2(z) = \frac{D_H^{0.5}}{8A_H^{2.5} z_g^2} \exp\left(-\frac{A_H z_g^2 + E_H z_g + C_H}{D_H}\right) \cdot \left\{2A_H^{0.5} D_H^{0.5}\left[E_H\left(-1\right.\right.\right.$$

$$+\exp\left(\frac{A_H z_g^2 + E_H z_g}{D_H}\right)\Bigg) + 2A_H z_g\Bigg] + \exp\left(\frac{\left(2A_H z_g + E_H\right)^2}{4A_H D_H}\right)\pi^{0.5}\left[-4A_H^2 z_g^2 + E_H^2 + 2A_H D_H\right]\left[\operatorname{erf}\left(\frac{E_H}{2A_H^{0.5} D_H^{0.5}}\right) - \operatorname{erf}\left(\frac{2A_H z_g + E_H}{2A_H^{0.5} D_H^{0.5}}\right)\right]\Bigg\} \tag{8}$$

$$\psi_3(z) = \frac{D_C^{0.5}}{8A_C^{2.5} z_g^2}\exp\left(-\frac{A_C z_g^2 + B_C z_g + C_C}{D_C}\right)\cdot\Bigg\{2A_C^{0.5} D_C^{0.5}\left[B_C\left(-1 + \exp\left(\frac{A_C z_g^2 + B_C z_g}{D_C}\right)\right) + 2A_C z_g\right] + \exp\left(\frac{\left(2A_C z_g + B_C\right)^2}{4A_C D_C}\right)\cdot\pi^{0.5}\left[-4A_C^2 z_g^2 + B_C^2 + 2A_C D_C\right]\left[\operatorname{erf}\left(\frac{B_C}{2A_C^{0.5} D_C^{0.5}}\right) - \operatorname{erf}\left(\frac{2A_C z_g + B_C}{2A_C^{0.5} D_C^{0.5}}\right)\right]\Bigg\} \tag{9}$$

$$\psi_4(z) = \frac{D_C^{0.5}}{8A_C^{2.5} z_g^2}\exp\left(-\frac{A_C z_g^2 + E_C z_g + C_C}{D_C}\right)\cdot\Bigg\{2A_C^{0.5} D_C^{0.5}\left[E_C\left(-1 + \exp\left(\frac{A_C z_g^2 + E_C z_g}{D_C}\right)\right) + 2A_C z_g\right] + \exp\left(\frac{\left(2A_C z_g + E_C\right)^2}{4A_C D_C}\right)\cdot\pi^{0.5}\left[-4A_C^2 z_g^2 + E_C^2 + 2A_C D_C\right]\left[\operatorname{erf}\left(\frac{E_C}{2A_C^{0.5} D_C^{0.5}}\right) - \operatorname{erf}\left(\frac{2A_C z_g + E_C}{2A_C^{0.5} D_C^{0.5}}\right)\right]\Bigg\} \tag{10}$$

$$A_H = \tau_0 + \tau''\left(1 + tg^2\gamma\right) \tag{11}$$

$$B_H = 2\left(\tau''\left(\xi + \nu\left(\tau'' + \tau_0\right)\right)tg\gamma - \left(\tau_0 + \tau''\right)z\right) \tag{12}$$

$$C_H = z^2\left(\tau_0 + \tau''\right) \tag{13}$$

$$D_H = 4a\tau''\left(\tau_0 + \tau''\right) \tag{14}$$

$$E_H = 2\left(\tau''\left(\xi + \nu\left(\tau'' + \tau_0\right)\right)tg\gamma + \left(\tau_0 + \tau''\right)z\right) \tag{15}$$

$$A_C = \tau_0 + \left(\tau - \tau'\right)\left(1 + tg^2\gamma\right) \tag{16}$$

$$B_C = 2\left(\left(\tau - \tau'\right)\left(x - \nu\tau' - x_0\right)tg\gamma - \left(\tau_0 + \tau - \tau'\right)z\right) \tag{17}$$

$$C_C = z^2\left(\tau_0 + \tau - \tau'\right) \tag{18}$$

$$D_C = 4a\left(\tau - \tau'\right)\left(\tau_0 + \tau - \tau'\right) \tag{19}$$

$$E_C = 2\left(\left(\tau - \tau'\right)\left(x - \nu\tau' - x_0\right)tg\gamma + \left(\tau_0 + \tau - \tau'\right)z\right) \tag{20}$$

$$\xi = x - \nu\left(\tau + \tau_0\right) - x_0 \tag{21}$$

$$\tau'' = \tau - \tau' \tag{22}$$

$\theta(x, y, z, \tau)$ denotes current temperature [°C]; θ_0, initial temperature [°C]; a, thermal diffusivity [m^2/s]; c, specific heat [J/(kgK]; ρ, density (kg/m^3); x_0, y_0, coordinates of the bead beginning [m]; x_f, coordinate of the bead end [m]; $l = x_f - x_0$, the weld length [m]; $\dot{q}$, heat source power [W] τ, time [s]; ν, heat source velocity [m/s]; γ [degrees], angle of electrode inclination defined as follows (see Figure 1):

$$\gamma = \beta - 90^\circ \tag{23}$$

t_0 [s] indicates quantity characterizing Gaussian power distribution on the overlayed surface, which is associated with the average radius r_B of power (see Figure 2) by relation [41]:

$$r_B^2 = 4a\tau_0 \tag{24}$$

3. Example of Calculations

The calculation of temporary temperatures in GMAW overlayed S235 steel plate has been conducted. The padding of a rectangular element (0.6 m x 0.4 m) was considered with a thickness of 0.03 m, which fulfills the conditions of the semi-infinite model of the body. Computation of temperature field was made for the padding weld applied along the long axis of the symmetry plate with the coordinates of the beginning and end of the bead $x_0 = 0.2$ m and $x_k = 0.4$ m, respectively.

The author's structural program, written in Borland Pascal, was used for computations. The thermal material properties were defined by $a = 8{\cdot}10^{-6}$ (m^2/s), $c = 670$ (J/(kg K)), and $\rho = 7800$ (kg/m^3); the average values of these properties in the temperature range from solidus to room temperature. In calculations current $I = 280$ A, voltage $U = 28$ V, and arc efficiency $\eta_e = 0.7$ have been assumed, which according to the formula

$$\dot{q} = \eta_e UI \tag{25}$$

allowed one to calculate the power of the source 5488 (W). Gaussian power distribution along its diameter and parabolic change into depth has been defined by $t_0 = 0.5$ s and $z_0 = 0.007$ m, respectively.

The temporary temperatures in the whole element for electrode tilt angles β =60°, 90°, and 120° (please compare Figure 1) with welding velocity $\nu = 0.007$ m/s have been calculated. Overall power of heat source was assumed to be constant for different inclination angles of the source.

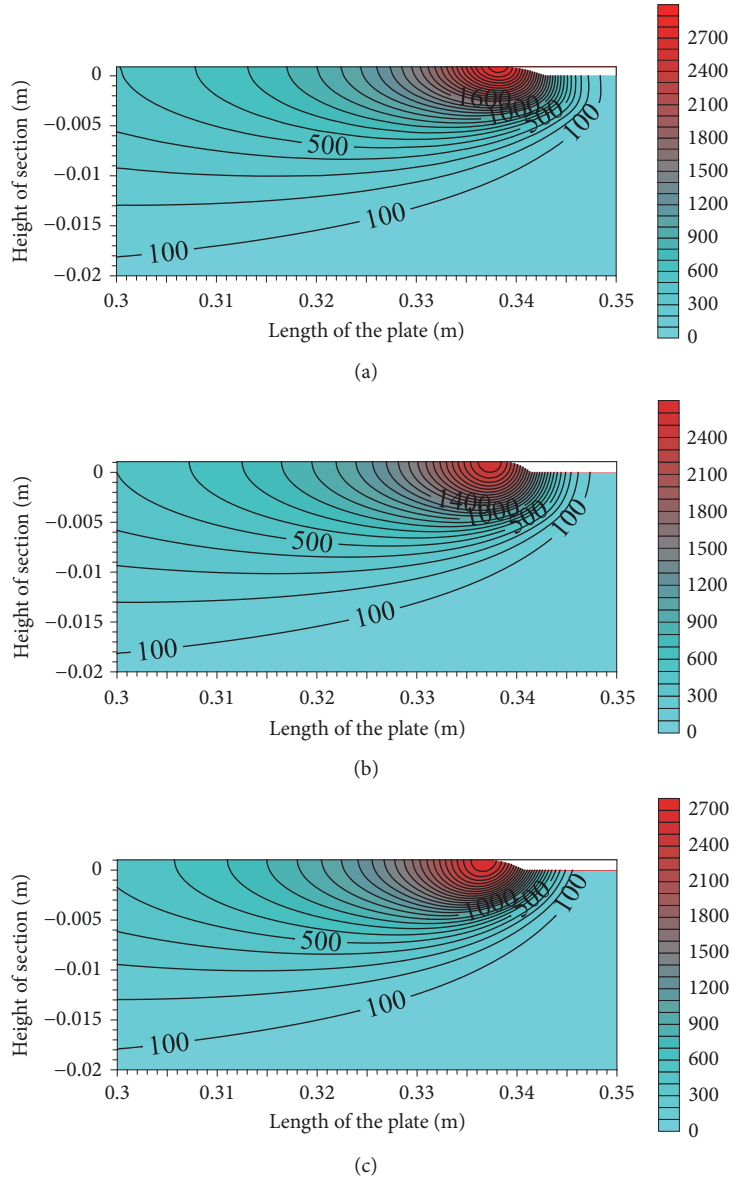

Figure 5: Temporary temperatures (°C) in longitudinal sections of plates: (a) $\beta = 60°$; (b) $\beta = 90°$; (c) $\beta = 120°$.

The temperature distribution in longitudinal sections, cross sections, and planes parallel to the surface of the plate has been analyzed. Since the largest temperature changes (fields with large gradients) in the HAZ were observed, a graphical illustration of the calculation results was limited to these areas. Detailed analysis was carried out for the position of the electrode specified by the coordinate $x = 0.34$ m. This position (at a distance of 0.14 m from the beginning of the bead) the electrode reaches at the time $\tau = 21$ s from the start of the weld overlaying process. Temporary temperature distributions in longitudinal sections are presented in Figure 5.

As you can see in Figure 5, the inclination of the electrode causes changes in the depth of material heating. For angle $\beta = 60°$, the temperature near the heat source is higher than in the other two cases. However, heating up to 500° is the deepest for angle $\beta = 120°$. The inclination of the electrode at an angle of $\beta = 60°$ causes the material before the electrode to be heated earlier than at the perpendicular position of the electrode and with the inclination to the opposite side. This is visible in the figure in the form of an isothermal shift to the right (in the direction of the electrode's movement) in comparison with the other two positions. The transient temperature distribution on the surface of the plate is shown in Figure 6, while in the plane it is 5 mm deeper, in Figure 7. When comparing the temperature distributions value for particular inclination electrode angles, one can notice an isotherm shift with the same temperature. This is clearly visible, especially in Figure 7.

Temporary temperature analysis was performed (Figure 8) for cross-sections specified by the coordinate $x = 0.34$ m and the electrode position specified by this coordinate. Temperatures at the point of the plate determined by the

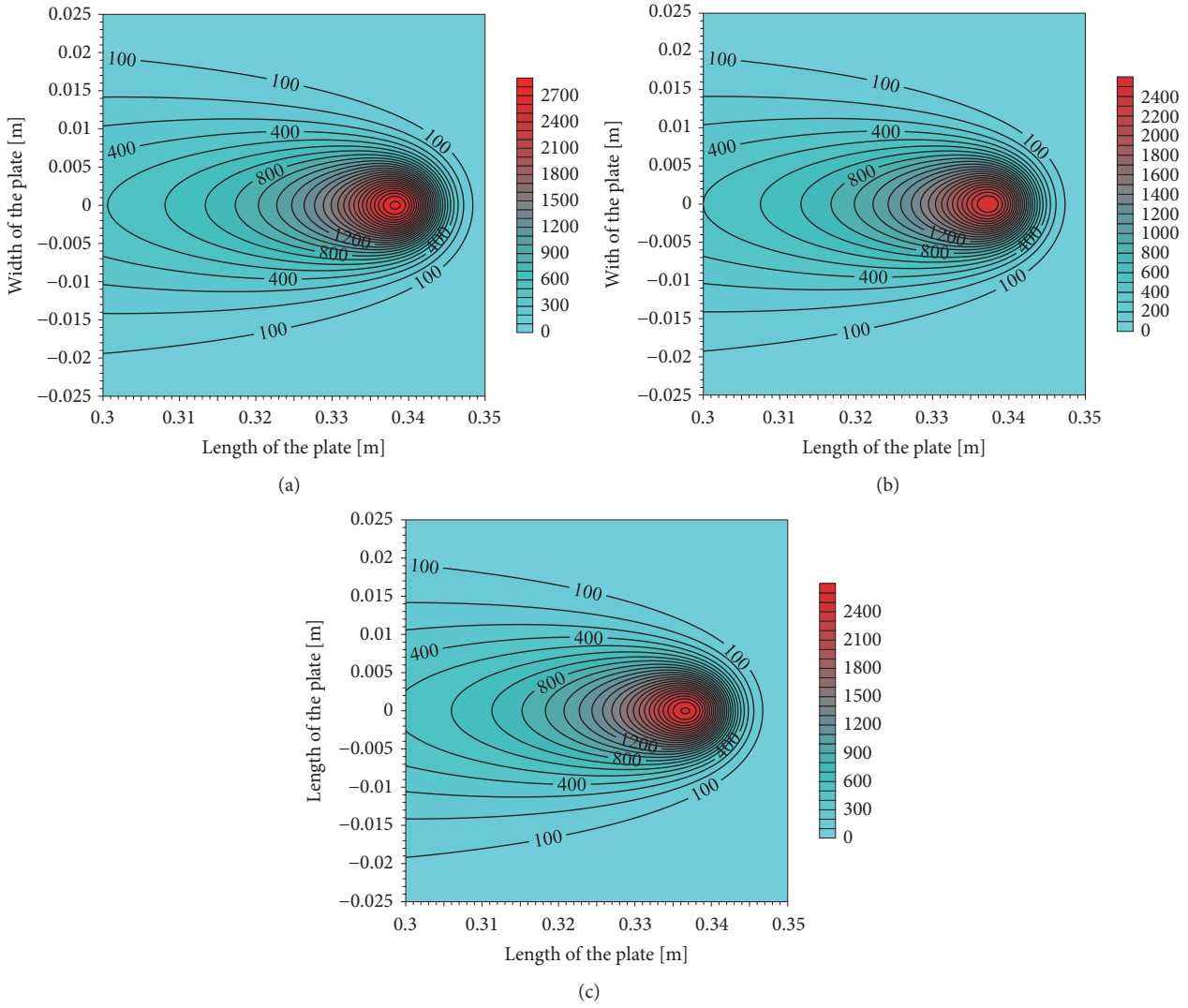

FIGURE 6: Temporary temperature (°C) on the surface of plates: (a) $\beta = 60^{\circ}$; (b) $\beta = 90^{\circ}$; (c) $\beta = 120^{\circ}$.

position of the electrode for angles $\beta = 60^{\circ}$, 90°, and 120° are equal to 2618.5°C, 2137.2°C, and 2027.9°C, respectively. The depth of the temperature field determined by the isotherm 100°C is similar to the angles $\beta = 60^{\circ}$ and $\beta = 90^{\circ}$, while at $\beta = 120^{\circ}$ the depth is smaller.

The maximum temperatures achieved in the cross-sections of the considered plates are compared in Figure 9. At the point located on the surface of the plate and in the axis of the weld, these values for angles $\beta = 60^{\circ}$, 90°, and 120° are equal to 2864°C, 2574.4°C, and 2683.6°C, respectively. The tilt of the electrode causes a decrease in the heating depth of the material to a certain temperature (e.g., 500 [°C], cf. Figures 8 and 9) when the maximum temperature on the plate surface is increased. The highest maximum temperature was calculated for the electrode inclined opposite to the direction of movement, while the smallest for the position perpendicular to the welded material.

The isotherms of maximum temperature allow for the determination of HAZ (heat affected zones) (Figure 10). The dimensions of these zones for particular angles of electrode inclination are summarized in Table 1. The largest widths of the zones (fusion, full and partial transformations) were measured for the angle $\beta = 60^{\circ}$, while the lowest for $\beta = 120^{\circ}$.

The history of temperature changes at the point of the considered cross-section, located in the weld axis on the top surface of the plate, in form of welding thermal cycle in Figure 11 is illustrated. Temperature peaks in thermal cycles for individual inclination angles are achieved at different times and they have different values. Table 2 shows the temperature values for selected times; the asterisk indicates the maximum temperature values in particular cycles. At time 21.25 s, the temperature during surfacing with the angle $\beta = 60^{\circ}$ is highest and 288.1°C higher than that of the angle $\beta = 90^{\circ}$ and 291.1°C higher than at the angle $\beta = 120^{\circ}$.

As the heat source moves, the temperature at the point under consideration decreases with $\beta = 60^{\circ}$, while in the other two cases it increases to the maximum. At time 21.5 s by the

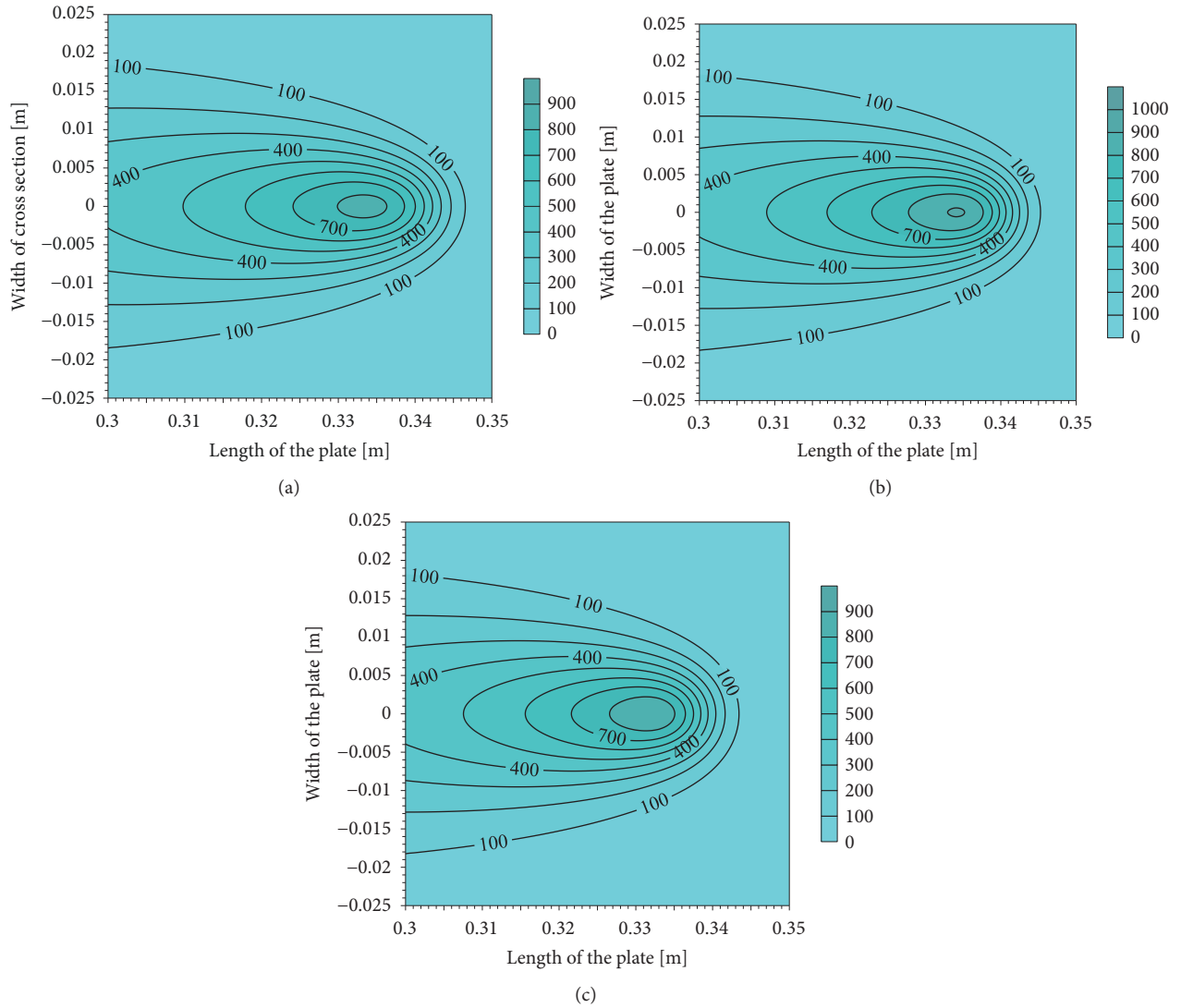

Figure 7: Temporary temperatures (°C) at the depth = 0.005 m from the surface of plates: (a) $\beta = 60^{\circ}$; (b) $\beta = 90^{\circ}$; (c) $\beta = 120^{\circ}$.

Table 1: Dimensions of HAZ (heat affected zones).

Dimension	$\beta = 60^{\circ}$	$\beta = 90^{\circ}$	$\beta = 120^{\circ}$
Width of fusion zone on surface of the plate ($z = 0$), [mm]	8.6	8	8.4
Depth of fusion zone ($y = 0$), [mm]	3	3.3	3.3
Width of full transformation zone on surface of the plate ($z = 0$), [mm]	13	12.6	12.8
Depth of full transformation zone ($y = 0$), [mm]	5	5.3	5.2
Total width (all heat affected zones) on surface of the plate ($z = 0$), [mm]	14.2	13.8	14
Total width (all heat affected zones) on surface of the plate ($y = 0$), [mm]	5.6	5.85	5.75

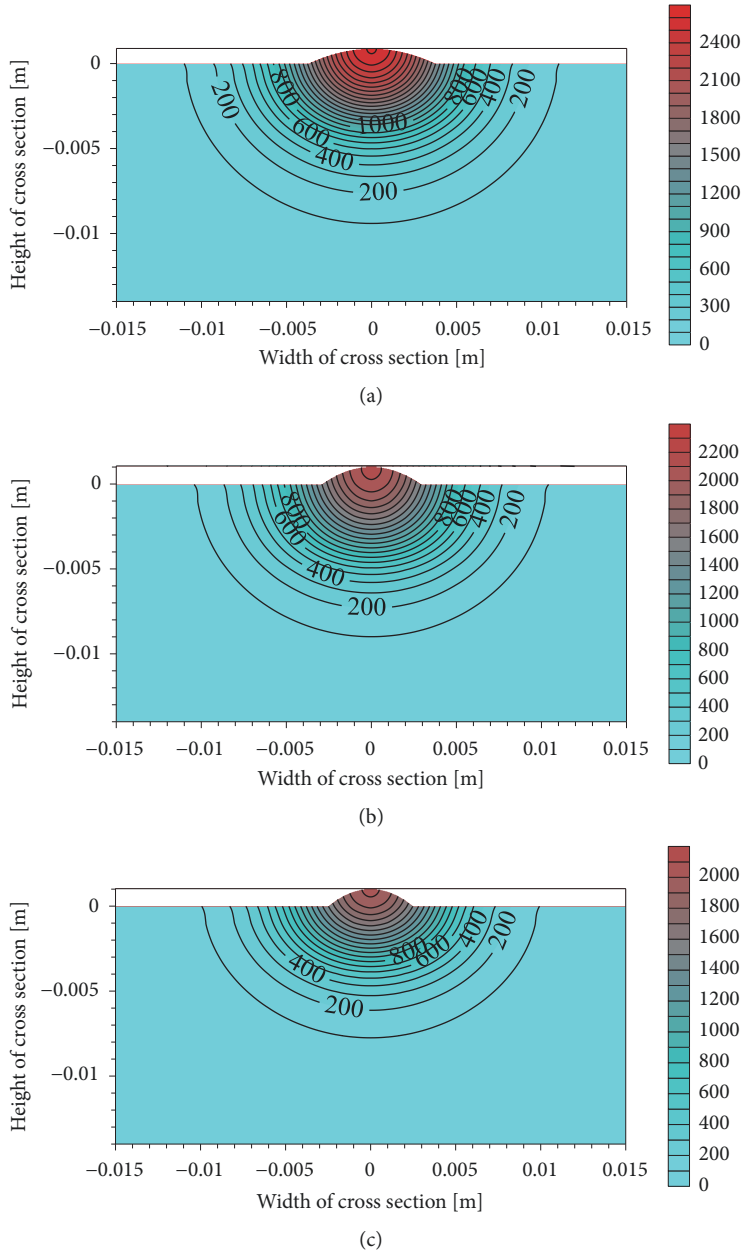

Figure 8: The temporary temperature (°C) distributions for electrode inclination angles: (a) $\beta = 60^{\circ}$; (b) $\beta = 90^{\circ}$; (c) $\beta = 120^{\circ}$.

Table 2: Temperatures at selected point for different tilt angles of electrode.

Time [s]	Temperature [°C]		
	$\beta = 60^{\circ}$	$\beta = 90^{\circ}$	$\beta = 120^{\circ}$
21.25	2730.9*	2442.8	2439.8
21.40	2683.4	2500.1*	2590.1
21.50	2599.7	2477.7	2619.9*

*Maximum temperature in the cycle.

angle $\beta = 120^{\circ}$ the temperature reaches a maximum value that is 20.2°C and 142.2°C higher than at the same time during surfacing with angles $\beta = 60^{\circ}$ and $\beta = 90^{\circ}$, respectively.

4. Summary and Conclusion

Modeling of the weld surfacing process involves the appropriate determination of the temperature field, the quantitative evaluation of the phase transformations, and the determination of the strains and temporary stresses (occurring in the surfacing process) and the residual stresses after the surfacing. A point of departure in the accepted modeling of the temperature field therefore is the adoption of a suitable heat source, the restoration of the corresponding electrode movement, and its position relative to the surfaced system.

The analysis of the results of the temperature field calculations for different angles of electrode inclination with respect

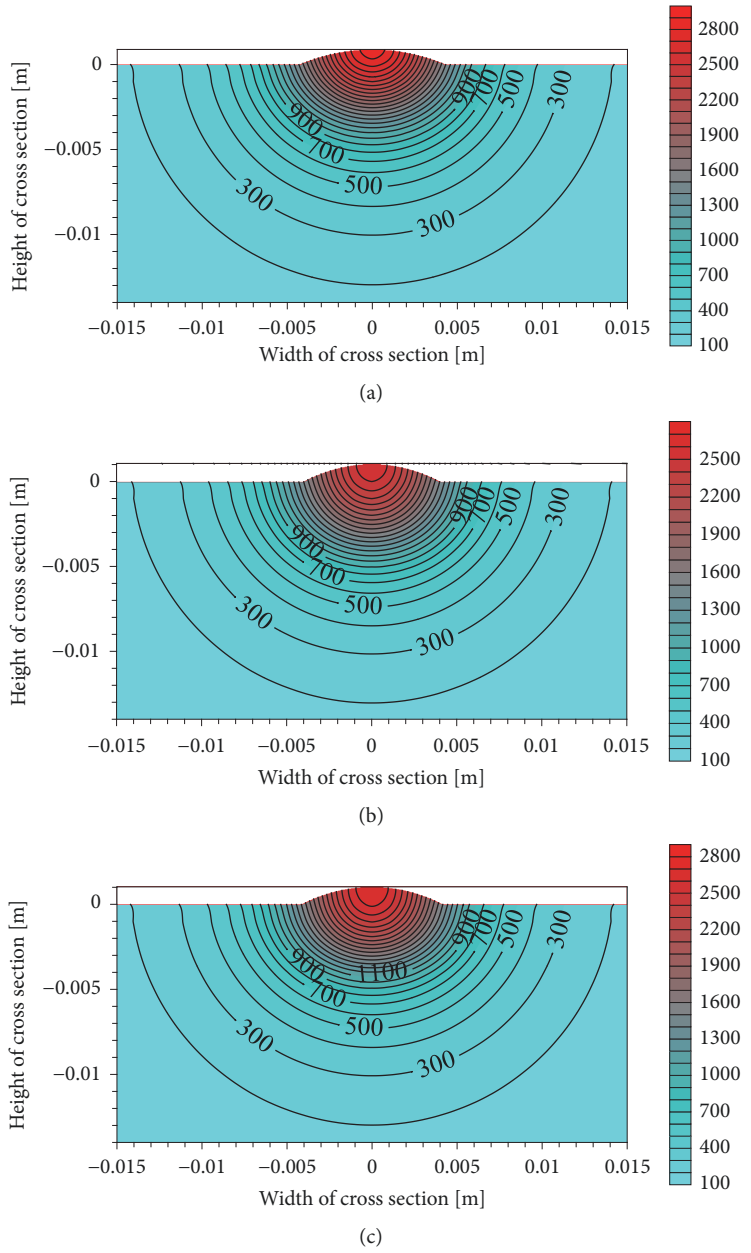

Figure 9: The maximum temperature (°C) distribution for electrode inclination angles: (a) $\beta = 60^{\circ}$; (b) $\beta = 90^{\circ}$; (c) $\beta = 120^{\circ}$.

to its motion direction allowed us to formulate the following conclusions.

(i) The electrode inclination reduces the depth of material heating. In the case of the tilt angle of the electrode $\beta = 60^{\circ}$ (opposite the velocity vector), a broader but shallower heat affected zone is obtained at significantly higher temperatures than for angle $\beta > 90^{\circ}$. For $\beta = 120^{\circ}$ (the tilt of the electrode according to its velocity vector) the dimensions of the HAZ, the narrowest and deepest HAZ are obtained for the angle $\beta > 90^{\circ}$.

(ii) When the electrode is tilted opposite to the electrode movement, the maximum temperature value is significantly higher than the inclined electrode in the direction of motion or perpendicular to the plate surface, and the isotherm face is shifted more toward the source movement than the other two cases.

In conclusion, it should be noted that the inclination of the electrode causes a decrease in the depth of its action. In the case of an electrode tilt, angle $\beta = 60^{\circ}$ produces a broader but shallower heat affected zone at significantly higher temperatures than for angles $\beta > 90^{\circ}$. $\beta = 120^{\circ}$; dimensions of the heat affected zone are intermediate, while the narrowest and deepest HAZ are obtained for the angle $\beta > 90^{\circ}$.

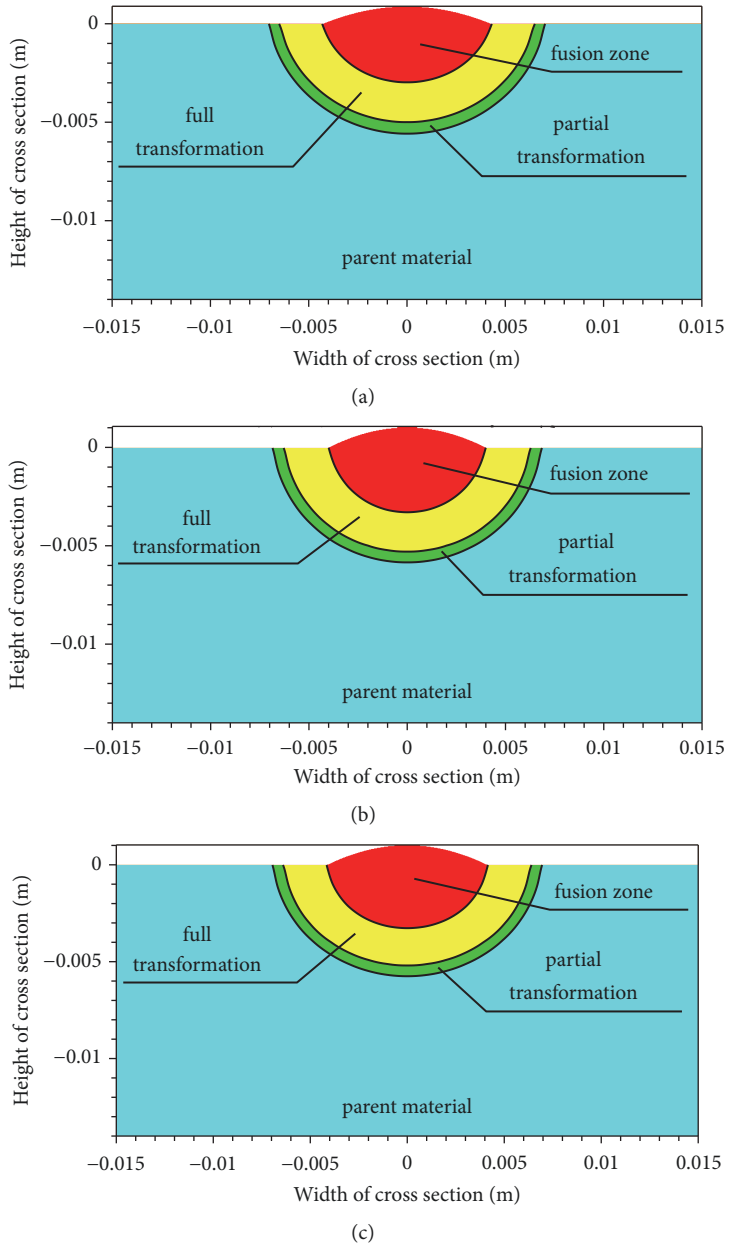

Figure 10: Heat affected zones for electrode inclination angles: (a) $\beta = 60^{\circ}$; (b) $\beta = 90^{\circ}$; (c) $\beta = 120^{\circ}$.

A further direction of the research will be the experimental verification of the developed theoretical model and a statistical test of the impact of the electrode's inclination on the geometric dimensions of the pads, as well as heat affected zones. It is also interesting to analyze the potential influence of the electrode's inclination (differentiated temperature distribution) on the material structure caused by phase transformations. The verified model of the temperature field and the inclusion of phase transformations will allow the analysis of deformation and stress states.

Nomenclature

a: Thermal diffusivity (m^2/s)
A_1: Temperature of austenitization beginning (°C)
A_3: Temperature of the austenitization end (°C)
C_p: Specific heat [J/kgK]
d: Diameter of electrode (m)
FEM: Finite Element Method
FCAW: Flux-Cored Arc Welding
FSW: Friction Stir Welding
GMAW: Gas metal arc welding
GTA: Gas Tungsten Arc
h: Reinforcement height (mm)
I: Current, amperage (A)
l: Padding weld length (m)
LBW: Laser beam welding
PAC: Plasma Arc Cutting
PAW: Plasma Arc Welding
SAW: Submerged arc welding

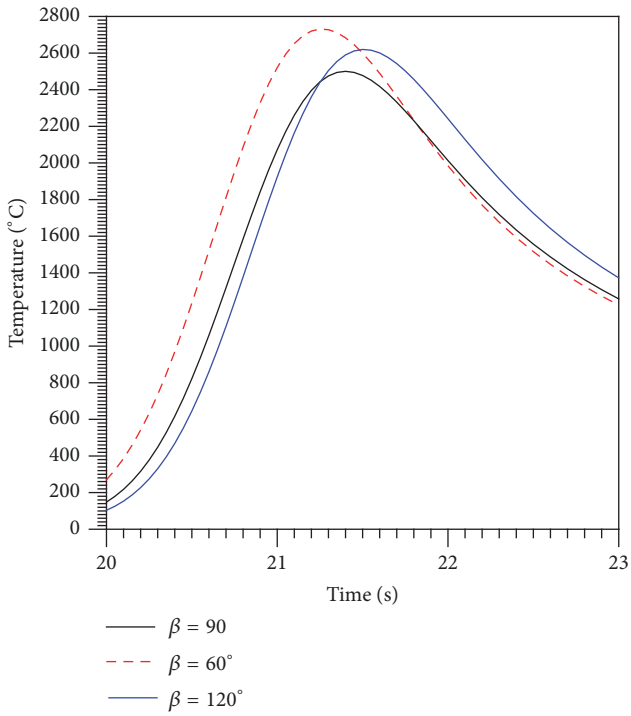

Figure 11: Thermal history at selected point.

TIG: Tungsten Insert Gas
U: Voltage (V)
v: Velocity of welding overlaying (m/s)
v_e: Wire feed speed (m/min)
p: Depth of penetration, fusion (mm)
x, y, z: Cartesian coordinates
w: Width of padding weld (mm).

Greek Letters

θ: Temperature of the material (K, °C)
θ_i: Initial temperature of the material (K, °C)
τ: Time (s)
η_e: Arc efficiency.

Data Availability

The data used to support the findings of this study are available from the corresponding author upon request.

Conflicts of Interest

The authors declare no conflicts of interest.

Acknowledgments

This research has been cofinanced by Czestochowa University of Technology and University of Žilina.

References

[1] W. Jiang, K. Yahiaoui, F. R. Hall, and T. Laoui, "Finite element simulation of multipass welding: full three-dimensional versus generalized plane strain or axisymmetric models," *Journal of Strain Analysis for Engineering Design*, vol. 40, no. 6, pp. 587–597, 2006.

[2] Y. Shim, Z. Feng, S. Lee et al., "Determination of residual stresses in thick-section weldments," *Welding Journal*, vol. 71, no. 9, pp. 305–312, 1992.

[3] H. X. Wang, J. S. Sun, Y. H. Wei, and Y. Y. Zheng, "Simulation of GMAW thermal process based on string heat source model," *Science and Technology of Welding and Joining*, vol. 10, no. 5, pp. 511–520, 2013.

[4] J. Hildebrand, I. Starcevic, F. Werner, H. Heinemann, and G. Köhler, "Numerical simulation of TIG-dressing of welded joints," in *Proceedings of Joint International Conference on Computing and Decision Making in Civil and Building Engineering*, pp. 1487–1496, Montreal, Canada, June 2006.

[5] S. H. Kang and H. S. Cho, "Analytical solution for transient temperature distribution in gas tungsten arc welding with consideration of filler wire," *Proceedings of the Institution of Mechanical Engineers, Part B: Journal of Engineering Manufacture*, vol. 213, no. 8, pp. 799–811, 1999.

[6] A. Ghosh, N. Barman, H. Chattopadhyay, and S. Hloch, "A study of thermal behaviour during submerged arc welding," *Strojniski Vestnik: Journal of Mechanical Engineering*, vol. 59, no. 5, pp. 333–338, 2013.

[7] M. M. Mahapatra, G. L. Datta, and B. Pradhan, "Three-dimensional finite element analysis to predict the effects of shielded metal arc welding process parameters on temperature distributions and weldment zones in butt and one-sided fillet welds," *Proceedings of the Institution of Mechanical Engineers, Part B: Journal of Engineering Manufacture*, vol. 220, no. 6, pp. 837–845, 2006.

[8] S. Joshi, J. Hildebrand, A. S. Aloraier, and T. Rabczuk, "Characterization of material properties and heat source parameters in welding simulation of two overlapping beads on a substrate plate," *Computational Materials Science*, vol. 69, pp. 559–565, 2013.

[9] A. Franco, L. Romoli, and A. Musacchio, "Modelling for predicting seam geometry in laser beam welding of stainless steel," *International Journal of Thermal Sciences*, vol. 79, pp. 194–205, 2014.

[10] W. Piekarska and M. Kubiak, "Three-dimensional model for numerical analysis of thermal phenomena in laser–arc hybrid welding process," *International Journal of Heat and Mass Transfer*, vol. 54, no. 23-24, pp. 4966–4974, 2011.

[11] A. Moarrefzadeh, "Numerical simulation of workpiece thermal profile in plasma arc cutting (PAC) process," *WSEAS Transactions on Applied and Theoretical Mechanics*, vol. 6, no. 4, pp. 160–166, 2011.

[12] Y. Li, Y. Feng, X. Zhang, and C. Wu, "An evolutionary keyhole-mode heat transfer model in continuous plasma arc welding," *International Journal of Heat and Mass Transfer*, vol. 117, pp. 1188–1198, 2018.

[13] M. Haghpanahi, S. Salimi, P. Bahemmat, and S. Sima, "3-D transient analytical solution based on Green's function to temperature field in friction stir welding," *Applied Mathematical Modelling*, vol. 37, no. 24, pp. 9865–9884, 2013.

[14] H. Jiang and H. Dai, "Effect of laser processing on three dimensional thermodynamic analysis for HSLA rectangular

steel plates," *International Journal of Heat and Mass Transfer*, vol. 82, pp. 98–108, 2015.

[15] O. V. Berezshnaya, E. P. Gribkov, and V. D. Kuznestov, "Investigation of thermostressed state coating formation at electric contact surfacing of Shaft type parts," *Advances in Materials Science and Engineering*, vol. 2016, Article ID 6597317, 14 pages, 2016.

[16] S. Feng, C. Huang, J. Wang, H. Zhu, P. Yao, and Z. Liu, "An analytical model for the prediction of temperature distribution and evolution in hybrid laser-waterjet micro-machining," *Precision Engineering*, vol. 47, pp. 33–45, 2017.

[17] Z. Murčinková and K. Vasilko, "Thermo-physical aspects of chip machining," *High Temperatures - High Pressures*, vol. 45, no. 4, pp. 273–289, 2016.

[18] D. Rosenthal, "Mathematical theory of heat distribution during welding and cutting," *Welding Journal*, vol. 20, no. 5, pp. 220s–234s, 1941.

[19] N. Rykalin, *Fundamentals of Heat Flow in Welding. AN SSSR*, Moskva, 1947.

[20] T. W. Eagar and N. S. Tsai, "Temperature fields produced by travelling distributed heat sources," *Welding Journal*, vol. 62, pp. 346s–355s, 1983.

[21] J. Goldak, A. Chakravarti, and M. Bibby, "A double ellipsoidal finite element model for welding heat source, II W Doc. No.212-603-85," 1985.

[22] S. K. Jeong and H. S. Cho, "An analytical solution to predict the transient temperature distribution in fillet arc welds," *Welding Journal*, vol. 76, no. 12, pp. 223s–232s, 1997.

[23] N. T. Nguyen, K. Matsuoka, N. Suzuki, and Y. Maeda, "Analytical solutions for transient temperature of semi-infinite body subjected to 3-D moving heat sources," *Welding Journal*, vol. 78, pp. 265s–274s, 1999.

[24] Y. Gu, Y. D. Li, Y. Yong, F. L. Xu, and L. F. Su, "Determination of parameters of double-ellipsoidal heat source model based on optimization method," in *Welding in the World*, pp. 1–12, 2009.

[25] C. Wu, Q. Hu, and J. Gao, "An adaptive heat source model for finite-element analysis of keyhole plasma arc welding," *Computational Materials Science*, vol. 46, no. 1, pp. 167–172, 2009.

[26] X. Jia, J. Xu, Z. Liu, S. Huang, Y. Fan, and Z. Sun, "A new method to estimate heat source parameters in gas metal arc welding simulation process," *Fusion Engineering and Design*, vol. 89, no. 1, pp. 40–48, 2014.

[27] Y. Mikami, T. Nakamura, and M. Mochizuki, "Numerical investigation of the influence of heat source modeling on simulated residual stress distribution in weaving welds," *Welding in the World*, vol. 60, no. 1, pp. 41–49, 2016.

[28] T. F. Flint, J. A. Francis, M. C. Smith, and J. Balakrishnan, "Extension of the double-ellipsoidla heat source model to narrow-groove and keyhole weld configurations," *Journal of Materials Processing Technology*, vol. 246, pp. 123–135, 2017.

[29] M. B. Nasiri and N. Enzinger, "An analytical solution for temperature distribution in fillet arc welding based on an adaptive function," in *Welding in the World*, pp. 1–11, 2018.

[30] C. Lv, G. Wang, H. Chen, and S. Wan, "Estimation of the moving heat source intensity using the multiple model adaptive inverse method," *International Journal of Thermal Sciences*, vol. 138, pp. 576–585, 2019.

[31] A. Klimpel, A. Czupryński, and A. Rzeźnikiewicz, "Influence of the direction and inclination angle of the GMA welding torch on the quality and technological properties of paddings made with cermet wire," *Welding Review*, vol. 77, no. 4-5, pp. 38–44, 2005.

[32] J. Pilarczyk, *Electrical Welding and Weld Overlaying of Metals*, Śląsk, Katowice, Poland, 2nd edition, 1996.

[33] A. Klimpel, M. Balcer, A. S. Klimpel, and A. Rzeźnikiewicz, "The effect of solid wire GMA weld surfacing technique and parameters on weld overlays quality and proportion of base material in weld overlay composition," *Institute of Welding Bulletin*, vol. 50, no. 1, pp. 53–58, 2006.

[34] L. Tuz and M. Mrozek, "The results of impact of the electrode lead angle on shape of the padding weld," *Mechanik*, vol. 85, no. 10, pp. 866–868, 2012.

[35] A. Kumar and T. DebRoy, "Heat transfer and fluid flow during gas-metal-arc fillet welding for various joint configurations and welding positions," *Metallurgical and Materials Transactions A: Physical Metallurgy and Materials Science*, vol. 38, no. 3, pp. 506–519, 2007.

[36] F. Hongyuan, M. Qingguo, X. Wenli, and J. Shude, "New general double ellipsoid heat source model," *Science and Technology of Welding and Joining*, vol. 10, no. 3, pp. 361–368, 2005.

[37] J. Chen, C. Wu, and M. Chen, "Improvement of welding heat source models for TIG-MIG hybrid welding process," *Journal of Manufacturing Processes*, vol. 16, no. 4, pp. 485–493, 2014.

[38] A. Ghosh, A. Yadav, and A. Kumar, "Modelling and experimental validation of moving tilted volumetric heat source in gas metal arc welding process," *Journal of Materials Processing Technology*, vol. 239, pp. 52–65, 2017.

[39] H. S. Carslaw and J. C. Jaeger, *Conduction of heat in solids*, Oxford University Press, Oxford, UK, 2nd edition, 1986.

[40] J. Winczek, "Analytical solution to transient temperature field in a half-infinite body caused by moving volumetric heat source," *International Journal of Heat and Mass Transfer*, vol. 53, no. 25-26, pp. 5774–5781, 2010.

[41] P. R. Vishnu, W. B. Li, and K. E. Easterling, "Heat flow model for pulsed welding," *Materials Science and Technology (United Kingdom)*, vol. 7, no. 7, pp. 649–659, 1991.